Structural Features of a Six-Nucleotide RNA Hairpin Loop Found in Ribosomal RNA†

Matthew A. Fountain,‡,§ Martin J. Serra,‖ Thomas R. Krugh,*,‡ and Douglas H. Turner*,‡

Department of Chemistry, University of Rochester, Rochester, New York 14627-0216, and Department of Chemistry, Allegheny College, Meadville, Pennsylvania 16335

Received November 10, 1995; Revised Manuscript Received March 4, 1996⊗

ABSTRACT: The hairpin loop GUAAUA occurs frequently in ribosomal RNA. Optical melting studies show that r(GGCGUAAUAGCC) folds into a hairpin containing this loop. The structural features of the r(GGCGUAAUAGCC) hairpin have been determined by NMR and molecular modeling. NOEs from G4-H1′ to A9-H2 and from A9-H2 to G10-H1′ show that G4 and A9 form a sheared base pair with two hydrogen bonds: A-N7 to G-NH_2 and A-NH6 to G-N3. One-dimensional NOE data show no NOEs between the imino protons of U5 and U8, but NOEs are observed between the U5-H1′ and the U8-H6 and U8-H5, thus orienting the U8 imino proton away from U5. Thus U5 and U8 do not form an imino hydrogen-bonded U·U pair. The U5-H2′ exhibits NOEs to both the A6-H8 and A7-H8, and the 3′ phosphorus resonances of U5 and A6 are shifted downfield. This suggests that the helix turn is between the U5 and A6 nucleotides. The $J_{H1'-H2'}$ and $J_{H3'-H4'}$ coupling constants indicate that the loop is dynamic, particularly at 35 °C, well below the melting temperature of 63 °C. Structures were generated using 75 distance and 46 dihedral angle restraints. In these structures, the U5 base is stacked on the sheared base pair formed by G4 and A9 and can initiate a uridine turn similar to that observed in the anticodon loop of tRNA. The A6, A7, and U8 bases can stack on one another with their hydrogen-bonding surfaces exposed to the solvent, suggesting that they are available for tertiary interactions or protein recognition in rRNA. A range of loop structures are consistent with the data, however. The lack of formation of a U·U mismatch is consistent with a recent model that predicts the stability of hairpin loops of six nucleotides on the basis of the closing base pair and first mismatch in the loop [Serra, M. J., Axenson, T. J., & Turner, D. H. (1994) *Biochemistry 33,* 14289−14296].

In addition to its roles in information transfer and regulation, RNA is associated with a host of cellular functions ranging from cleavage and ligation of nucleic acids (Cech, 1990; Altman, 1990; Pace & Brown, 1995; Luan et al., 1993) to protein transport across membranes (Walter & Blobel, 1982; Walter & Johnson, 1994). Despite its importance, relatively little is known about the three-dimensional structures of natural RNAs. Transfer RNA is the only natural RNA for which crystal structures are known (Kim et al., 1974; Robertus et al., 1974; Westhof et al., 1985). In addition, three-dimensional structures have been determined for a number of motifs found in larger RNAs (Szewczak et al., 1993; Cheong et al., 1990; Heus & Pardi, 1991; Wimberly et al., 1993; SantaLucia & Turner, 1993; Pley et al., 1994a; Scott et al., 1995; Puglisi et al., 1992; Ebel et al., 1994; Borer et al., 1995; Jaeger & Tinoco, 1993). Even secondary structures that are definitively known are rather scarce. These usually rely on sequence comparisons and thus require a large data base of sequences with identical function (Woese & Pace, 1993; Gutell et al., 1994; Michel & Westhof, 1990). To fill these gaps, methods are being developed to model the secondary and three-dimensional structures of RNA (Zuker, 1989; Turner et al., 1988; Gautheret et al., 1993; Michel & Westhof, 1990). Additional structural information is required for continued development and testing of these methods.

In this paper, NMR and molecular modeling are used to derive a structure for the RNA hairpin, G1-G2-C3-G4-U5-A6-A7-U8-A9-G10-C11-C12, shown in Figure 1. The six nucleotides underlined are a highly conserved sequence in the L11 protein binding region of the large subunit ribosomal RNA (Xing & Draper, 1995; Gutell et al., 1993). The first mismatch in the loop is GA, a common feature of many small hairpins (Woese et al., 1990; Heus & Pardi, 1991), which is known to contribute 0.7 kcal/mol to folding stability (SantaLucia et al., 1992; Serra et al., 1994).

MATERIALS AND METHODS

Sample Preparation. The RNA sequence r(GGCGUAAUAGCC) was synthesized using the phosphoramidite method (Usman et al., 1987). After ammonia and fluoride deprotection, the oligomer was purified by HPLC using a preparative PRP-1 reverse-phase column. The buffer for optical melting and NMR experiments was 0.1 M NaCl, 0.01 M sodium phosphate (pH 7.0), and 0.5 mM EDTA. The concentration of oligomer for NMR experiments was 1.8 mM.

Melting Curves and Data Analysis. Oligomer concentration was varied over a 1000-fold range with the highest concentration being 0.9 mM. Absorbance versus temperature was measured at 280 nm with a heating rate of 1.0 °C min^{-1}

† This publication was supported by NIH Grants GM53826 (T.R.K.), GM22939 (D.H.T.), and GM49429 (M.J.S.).

* Author to whom correspondence should be addressed.

‡ University of Rochester.

§ Present address: Hobart and William Smith Colleges, Geneva, NY 14456.

‖ Allegheny College.

⊗ Abstract published in *Advance ACS Abstracts,* May 1, 1996.

S0006-2960(95)02697-3 CCC: $12.00

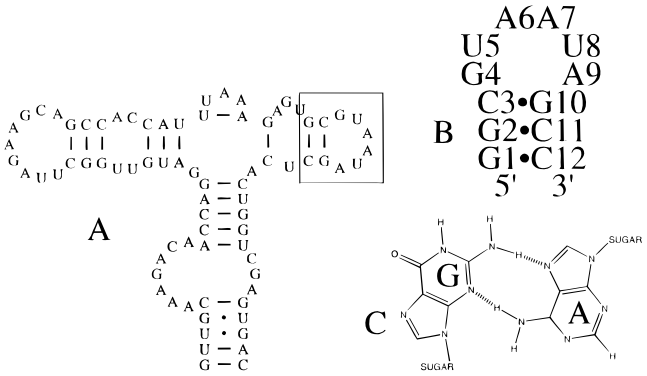

FIGURE 1: (A) Schematic of the secondary structure of the conserved L11 protein binding region of *Bacillus stearothermophilus* rRNA. (B) The hairpin studied by NMR and molecular modeling. (C) Schematic of a G·A mismatch.

on a Gilford 250 spectrophotometer as described previously (Freier et al., 1983; Petersheim & Turner, 1983). Absorbance versus temperature profiles were fit to a two-state model with sloping base lines using a nonlinear least squares program adapted for a unimolecular transition.

NMR Experiments. A Varian VXR 500S NMR spectrometer operating at 499.8 MHz (^{1}H) was used for all NMR experiments. NMR data were processed with VNMR (Varian) and FELIX 2.10 (Biosym Technologies Inc.) on Silicon Graphics, Inc., workstations. NOESY spectra were recorded with the standard $(90°-t_1-90°-\text{mix}-90°-\text{acquire})_n$ pulse sequence consisting of 256 t_1 increments, each having 2K points with 32 scans per fid and a recycle delay time of 3 s. The residual HOD peak was suppressed by irradiation during the recycle delay time. The data were zero filled to 2K data points in the t_1 dimension to yield a 2K by 2K matrix. The data were apodized with a shifted sine bell squared function in both dimensions.

TOCSY spectra were recorded using the standard $(90°-t_1-\text{spin lock}-\text{acquire})_n$ pulse sequence consisting of 256 t_1 increments each having 2K data points with either 64 or 96 transients per fid with a recycle delay time of 3 s and spin-lock mixing times of 50, 90, and 145 ms. The residual HOD peak was suppressed by irradiation during the recycle delay time. The data were zero filled to 2K data points in the t_1 dimension to yield a 2K by 2K matrix. The data were apodized with a phase-shifted sine bell squared function in both dimensions.

DQF-COSY and ^{31}P decoupled DQF-COSY spectra were acquired by the standard $(90°-t_1-90°-\tau-90°-\text{acquire})_n$ pulse sequence consisting of 256 t_1 increments, each having 4K data points. Typical data sets consisted of 32 or 64 scans per fid, with a 2.5 s recycle delay time. The data were apodized with a shifted sine bell squared function in both dimensions. WALTZ-16 decoupling was employed during the acquisition time for the ^{31}P decoupled DQF-COSY.

Proton-detected ^{1}H−^{31}P 2D heteronuclear correlation experiments (HETCOR) described by Sklenar et al. (1986) were performed with an inverse detection probe (Nalorac Inc.). Typical data sets consisted of 32 or 64 transients per fid, with a 1.0 s recycle delay time. A total of 256 t_1 increments with 2K data points each were used. A 2000 Hz sweep width was used in both the proton and phosphorus dimensions. Spectra were apodized with a phase shifted sine bell squared function in both dimensions.

Phase-sensitive NOESY experiments in H_2O were recorded with 100 and 150 ms mixing times at 10 °C, with a 1−1−echo water suppression pulse sequence replacing the last 90° pulse in the NOESY pulse sequence (Sklenar & Bax, 1987). A sweep width of 12 000 Hz was used in both dimensions with delays in the 1−1−echo water suppression pulses of 50 μs between the two 180° pulses and 80 ms for the echo delay. A total of 256 complex t_1 increments each having 4K data points were recorded using either 64 or 96 transients per t_1 increment and a recycle delay time of 3 s. The data were zero filled to 4K data points in the t_1 dimension to yield a 4K by 4K matrix. The data were apodized with a shifted sine bell squared function in both dimensions.

NOE Distance Measurements. NOE-derived distances were calculated from the ratio of the volume of the cross-peak in question to the average volume of the C11 and C12 H5−H6 cross-peaks using the isolated spin pair approximation, where the NOESY cross-peak volume is inversely proportional to the sixth power of the distance. Distances were calculated from a 120 ms mixing time NOESY spectrum collected at 25 °C.

Scalar Coupling Measurements. Proton−proton coupling values were measured in a high-resolution (1 Hz/point) ^{31}P decoupled DQF-COSY spectrum recorded at 25 °C. The average sugar proton line width was 3 Hz. Thus weak or absent coupling was assumed to be less than 3 Hz. H3′−P coupling was determined by subtracting the passive $J_{H2'-H3'}$ coupling from the H3′−P coupling obtained from a ^{1}H−^{31}P HETCOR spectrum recorded at 25 °C. In most cases, the $J_{H1'-H2'}$, $J_{H2'-H3'}$, $J_{H3'-H4'}$, and $J_{H3'-P}$ coupling constants were measured for each nucleotide. The torsion angles were determined from these values using the generalized Karplus equation (Haasnoot et al., 1980; Lankhorst et al., 1984). Dihedral restraints were given generous lower and upper bounds, typically ±30° or 40°, to acknowledge the possible impact of conformational averaging.

Structural Modeling. Insight II version 2.1.0 and Discover version 2.8 (Biosym Technologies Inc.) software packages on a Silicon Graphics workstation were used for graphics display and for computations using the AMBER force field (Singh et al., 1988; Weiner & Kollman, 1981; Weiner et al., 1984, 1986; Cornell et al., 1995). The AMBER force field parameters reported by Cornell et al. (1995) were used for all calculations. Phosphate oxygen charges were reduced by 50%, giving each nucleotide a net charge of −0.174. Calculations were done *in vacuo* with a nonbonding cutoff distance of 15 Å and a distance-dependent dielectric constant of $4.0R_{ij}$. The RNA hairpin was constructed from a single strand of A-form RNA by adjusting backbone dihedral angles in the loop so that the stem nucleotides would form a double helix after restrained energy minimization. The distance restraint penalty function consisted of a five-section continuous function:

$$E = \begin{cases} E_1 + (R_1 - R_{ij})F_1 & R_{ij} < R_1 \\ K_2(R_{ij} - R_2)^2 & R_1 < R_{ij} \le R_2 \\ 0 & R_2 < R_{ij} \le R_3 \\ K_3(R_{ij} - R_3)^2 & R_3 < R_{ij} \le R_4 \\ E_1 + (R_{ij} - R_4)F_4 & R_4 < R_{ij} \end{cases} \quad (1)$$

where R_1 and R_4 are the distances where the distance restraint

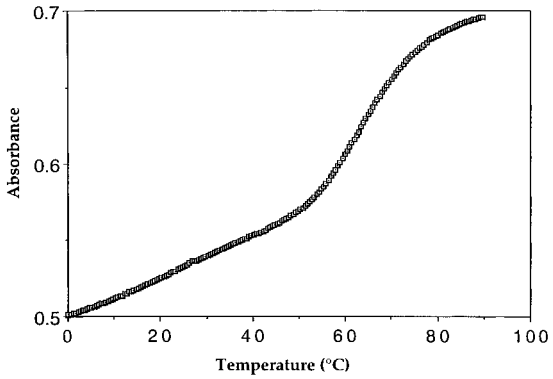

FIGURE 2: Melting profile at 280 nm of r(GGCGUAAUAGCC) at 0.9 mM. The melting buffer was 0.1 M NaCl, 0.01 M sodium phosphate, and 0.5 mM EDTA at pH 7.0.

penalty energy (E) is 1000 kcal/mol and the harmonic potential becomes linear, R_2 is the lower bound distance, R_3 is the upper bound distance, R_{ij} is the current distance between the two atoms, and F_1, F_4, K_2, and K_3 are force constants. The force constants K_2 and K_3 were set to 50 kcal mol^{-1} Å^{-2} for individual restraints, while F_1 and F_4 were set to 1000 kcal mol^{-1} Å^{-1} for all restraints. The force constants for dihedral angle restraints were 100 kcal mol $^{-1}$ rad^{-2}. Hydrogen bond restraints with bounds of 1.5−2.0 Å between each donor and acceptor were also employed for the G1·C12, G2·C11, and C3·G10 Watson−Crick base pairs to ensure the base pairing observed in the NMR spectra. No hydrogen-bonding restraints were used in the loop of the hairpin.

Calculations began with restrained energy minimization followed by 20 ps of restrained molecular dynamics with electrostatic charges turned off. Molecular dynamics were run at 300 K with a 0.001 ps time step and velocities randomized at the beginning. The nonbonding terms were scaled to 10% of their normal value at the start of the MD simulation. As the molecular dynamics simulation progressed, the nonbonding terms were gradually increased to their normal value. After molecular dynamics, charges were turned on and restrained energy minimization was resumed to provide an energy-minimized structure. Finally, all but the hydrogen-bonding restraints were removed, and energy minimization was performed to determine whether any significant changes in conformation occurred. The above procedure was repeated 30 times to generate structures that fit the NMR data.

RESULTS

Absorbance versus Temperature. UV melting experiments were used to determine whether the oligomer was forming a hairpin or duplex at NMR concentrations and to define the temperature range suitable for NMR. A typical absorbance versus temperature curve is shown in Figure 2. The melting temperature of 63 °C was concentration independent, as expected for unimolecular hairpin formation (Figure S1 of Supporting Information; see paragraph at end of paper regarding Supporting Information). The thermodynamic parameters for the hairpin transition are $\Delta H° = -32.8 \pm 2$ kcal/mol, $\Delta S° = 98 \pm 4$ eu, and $\Delta G_{37}° = -2.4 \pm 0.3$ kcal/mol. These are within experimental error of values previously reported for 0.1 M NaCl (Serra et al., 1994).

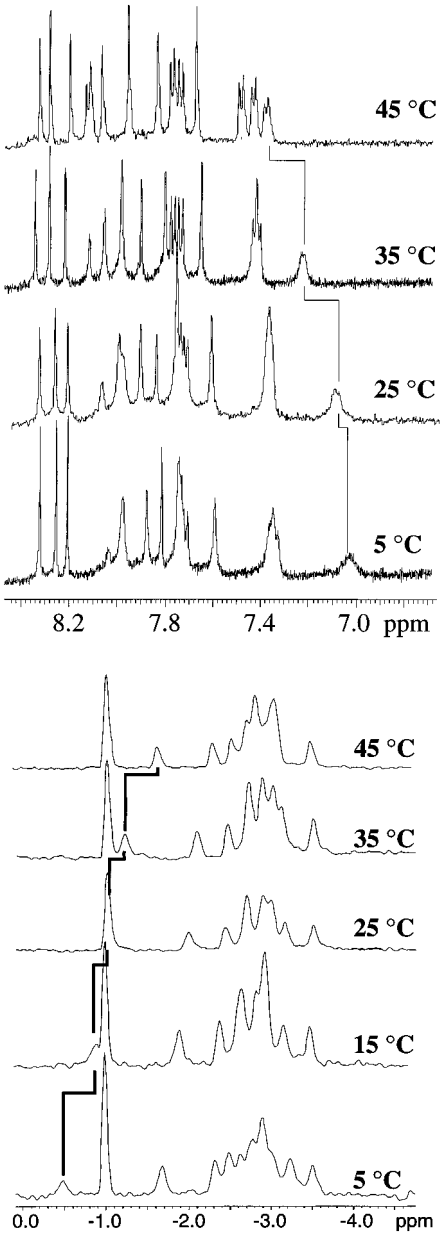

FIGURE 3: (Top) One-dimensional 500 MHz proton NMR spectra recorded in D_2O at 5, 25, 35, and 45 °C. The buffer was 0.1 M NaCl, 10 mM sodium phosphate, and 0.5 mM EDTA, pH 7.0. The U8-H6 resonance is traced. (Bottom) One dimensional phosphorus NMR spectra at 5, 15, 25, 35, and 45 °C.

Temperature Studies by NMR. Figure 3 shows one-dimensional spectra for the base proton region and for phosphorus at temperatures ranging from 5 to 45 °C. Chemical shift changes are observed in the base and sugar region and for certain phosphorus resonances far below the melting temperature of the hairpin. The U8 base and sugar proton resonances shift upfield as temperature is lowered. At temperatures below 20 °C, the U8 and U5 proton resonances begin to broaden, suggesting that conformational exchange between multiple conformers has slowed. Unfortunately, conformational exchange could not be slowed sufficiently to observe individual conformers. The U5, A6, and A7 base proton resonances have chemical shifts that are relatively independent of temperature, suggesting they are undergoing either small conformational changes or fast conformational interconversion between conformers. In a similar way, there are large temperature dependences of the

resonances for the phosphorus nuclei between U5 and A6 and between A6 and A7. Therefore, the structural features deduced for the hairpin loop must be considered those of an averaged structure. Distance and angle restraints were obtained from NMR data collected at 25 °C because this temperature afforded the best spectral dispersion of the sugar proton resonances for making assignments by correlation spectroscopy.

Exchangeable Proton Assignments. One-dimensional NOEs and chemical shift arguments were used to distinguish between the stem and loop imino protons. The six imino protons in the r(GGCGUAAUAGCC) hairpin are observed as well-resolved resonances in the one-dimensional spectrum recorded at −3 °C (spectrum A in Figure 4). Chemical shift comparisons with the r(GGCGAGCC)$_2$ duplex studied by SantaLucia and Turner (1993) suggest that the three downfield resonances are the stem G1, G2, and G10 imino protons. The terminal G1 imino proton was assigned to the broad resonance at 12.65 ppm due to the broadness associated with terminal imino protons and from the chemical shift comparison with r(GGCGAGCC)$_2$. One-dimensional NOE experiments (spectra B and C in Figure 4) show that the sharp resonances at 13.27 and 13.1 ppm originate from imino protons that are adjacent to one another, presumably the G2 and G10 imino protons. The three upfield resonances at 10.95, 10.75, and 10.57 ppm belong to the G4, U5, and U8 imino protons. Unequivocal resonance assignments for the G4, U5, and U8 imino protons could not be made due to the lack of sequential NOEs in both one- (spectra D and E in Figure 4) and two-dimensional NMR spectra recorded in 90:10 H_2O:D_2O solution (data not shown).

In internal loops of tandem U·U hydrogen-bonded mismatches, the two imino protons are close to one another and exhibit very strong NOEs to each other (SantaLucia et al., 1991; Nikonowicz & Pardi, 1992, 1993; Wu et al., 1995). The lack of observable NOEs between the upfield-shifted imino protons in Figure 4 suggests that U5 and U8 are not base paired as in internal loops of tandem U·U mismatches. One of the sharp resonances may be the G4 imino. A similarly placed G in a GCAA tetraloop exhibits a sharp resonance (Heus & Pardi, 1991), which has been suggested as reflecting a water-bridged hydrogen bond to phosphate (SantaLucia et al., 1992). NOEs between the U5-H1′ and U8-H5 and U5-H1′ and U8-H6 clearly indicate that a U·U base pair is not forming (see below). In fact, these NOEs place the U5 imino close enough to the phosphate between A7 and U8 to hydrogen bond directly, or via a water molecule, to this phosphate oxygen. This type of interaction is similar to the uridine turn motif observed in tRNA (Kim & Sussman, 1976; Quigley & Rich, 1976) and the hammerhead ribozyme (Pley et al., 1994; Scott et al., 1995).

Nonexchangeable Proton Assignments. Nonexchangeable proton assignments were made by previously described methods (Varani & Tinoco, 1991; Wüthrich, 1986). Due to spectral overlap, some chemical shift assignments were made or confirmed at other temperatures. Table 1 summarizes the chemical shift assignments at 25 °C (assignments obtained at other temperatures are noted).

The base to H1′ and H5 proton region of the 600 ms NOESY spectrum recorded at 25 °C is shown in Figure 5. The uracil and cytosine H5 and H6 resonances were assigned by inter- and intranucleotide NOEs and by their strong coupling cross-peaks in DQF-COSY and TOCSY spectra.

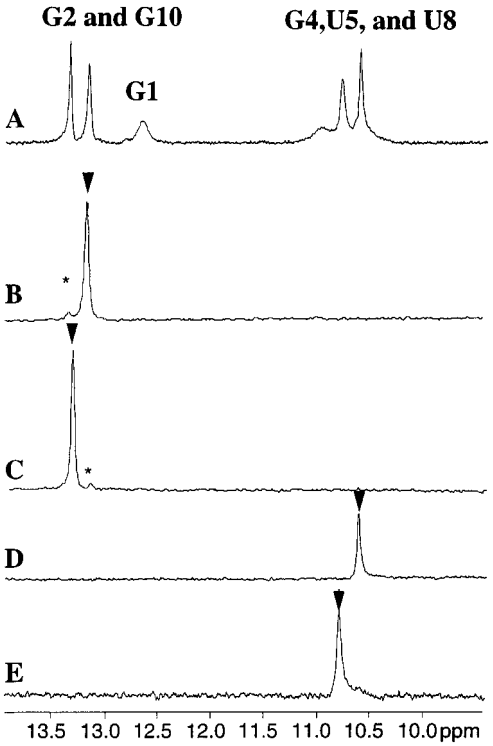

FIGURE 4: (A) One-dimensional 500 MHz proton NMR spectrum of the imino proton resonances recorded in H_2O. The buffer was 0.1 M NaCl, 10 mM sodium phosphate, and 0.5 mM EDTA in H_2O at pH 7.0. Spectra B, C, D, and E are difference spectra with the resonances denoted with a filled arrowhead irradiated for 2 s to provide saturation. Observed NOEs are designated by asterisks.

Table 1: Chemical Shift Assignments (ppm) for the Nonexchangeable Proton Resonances in the r(GGCGUAAUAGCC) Hairpin[a]

nucleotide	base	H1′	H2′	H3′	H4′	H5/H2	P[d]
G1	8.01	5.75	4.89	4.59	4.41		−2.98
G2	7.61	5.93	4.64	4.63	4.55		−2.94
C3	7.37	5.55	4.71	4.39	4.48	5.15	−3.17
G4	7.94	5.8	4.22	4.75	4.48		−2.71
U5	7.36	5.21	4.60	4.46	4.36	5.14	−0.89
A6	8.21	5.76	4.79	4.65	4.34	7.82	−1.93
A7	7.87	5.88	4.53	4.9	4.41	8.16	−3.19
U8	7.10	5.17	4.38	4.5	4.09	5.1	−3.04
A9	7.93	5.77	4.9	4.58	4.43	8.26	−2.87
G10	7.73[b]	4.72[b]	4.44	4.42	*c*		−3.5
C11	7.70[b]	5.58[b]	4.36	4.49	*c*	5.28	−2.51
C12	7.72[b]	5.78[b]	4.10	4.23	*c*	5.59	

[a] Assignments were made at 25 °C and referenced to the water resonance at 4.80 ppm except where indicated. [b] Chemical shift assignments were made at 35 °C. [c] Assignments were not possible due to spectral overlap. [d] P assignments are to the 5′ nucleoside.

The base to H1′ connectivities were made by comparison of the base to H1′ region of NOESY spectra collected at 25, 35, and 40 °C. In Figure 5, the base to H1′ NOE connectivities are traced with labels at the intranucleotide base to H1′ NOESY cross-peaks. The G10-H1′ proton at 4.72 ppm is upfield in the crowded sugar proton region of the spectrum, and alternate methods were used to make this assignment. G10-H1′ was assigned from NOESY cross-peaks to the C11-H6, G10-H8, and G10-H2′ in 600 ms NOESY spectra recorded at 35 and 40 °C (Figure S2 in Supporting Information). G10-H2′ was assigned by its strong NOE to the adjacent C11-H6 and to G10-H1′. To confirm the G10-H1′ assignment, the C11 and A9 sugar protons were

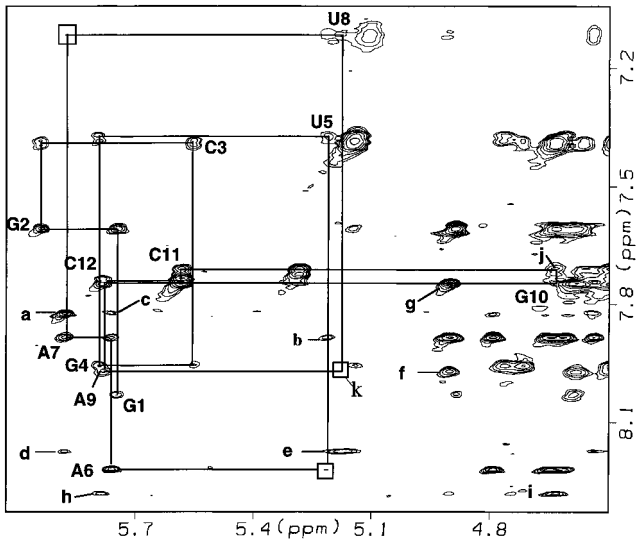

FIGURE 5: Base to H1′, H2, and H5 region of a 600 ms NOESY spectrum recorded at 25 °C in 0.1 M NaCl, 10 mM sodium phosphate, and 0.5 mM EDTA at pH 7.0. The base to H1′ NOESY walk is traced with solid lines with labels representing intranucleotide base to H1′ NOE connectivities. The labeled cross-peaks are (a) A6-H2 to A7-H1′, (b) A7-H8 to U5-H1′, (c) A6-H2 to A6-H1′, (d) A7-H2 to A7-H1′, (e) A7-H2 to U8-H1′, (f) A9-H3′ to A9-H8, (g) A9-H3′ to G10-H8, (h) A9-H2 to G4-H1′, (i) A9-H2 to G10-H1′, (j) G10-H1′ to C11-H6, and (k) U8-H1′ to A9-H8.

assigned to determine whether the resonance at 4.72 ppm belonged to these protons. Neither the A9 nor C11 sugar protons resonate at 4.72 ppm. Thus this resonance is assigned to G10-H1′.

All of the intranucleotide base to H1′ NOESY cross-peak intensities are weaker than the U and C H5/H6 cross-peaks, verifying that all of the bases are *anti*. If a base were in a *syn* conformation, the base to H1′ distance would be equal to or less than that of the C-H5/H6 distance, thus exhibiting a cross-peak that would be equivalent to or stronger than the C-H5/H6 cross-peak.

The A6, A7, and A9-H2 protons were distinguished from other base protons by their long T_1 relaxation times and their intranucleotide NOEs to H1′ protons. The A6-H2 and A7-H2 protons were distinguished from one another by NOEs to their own H1′ sugar protons, as shown in Figure 5. The A6-H2 proton exhibits NOEs to both A6-H1′ and A7-H1′ protons (cross-peaks c and a in Figure 5), whereas A7-H2 exhibits NOEs to A7-H1′ and U8-H1′ (cross-peaks d and e in Figure 5). Both A6-H2 and A7-H2 exhibit NOEs to A7-H1′, suggesting that the A6 and A7 bases are stacked. The adenine-H2 proton resonating at 8.32 ppm was assigned to A9-H2 on the basis of NOEs to the G10-H1′ and the G4-H1′ protons, which are adjacent to and opposite the A9 nucleotide, respectively (cross-peaks h and i in Figure 5). Interestingly, in order for these NOEs to occur, the A9 base must be partially displaced into the minor groove. The large upfield shift of the G10-H1′ proton is consistent with A9 being displaced and lying over the G10-H1′ proton. These NOEs suggest that G4 and A9 form a sheared base pair, as shown in Figure 1.

The H2′, H3′, and H4′ sugar proton assignments were primarily made from through-bond coupling interactions observed in TOCSY and DQF-COSY spectra and by NOEs between the H1′ and H2′ protons. Assignments of G10 sugar protons were made from NOEs to G10-H8 and C11-H6.

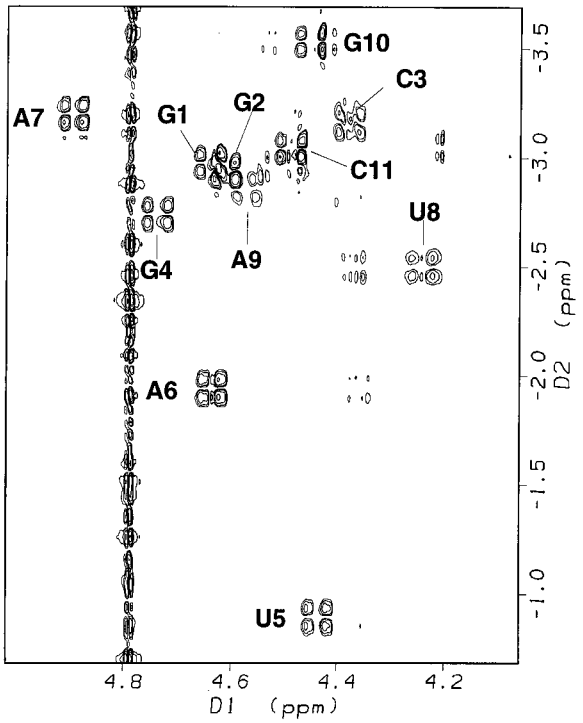

FIGURE 6: Proton−phosphorus HETCOR spectrum recorded at 25 °C in 0.1 M NaCl, 10 mM sodium phosphate, and 0.5 mM EDTA (pH 7.0). The phosphate resonances were referenced to 0.0 ppm. Peaks corresponding to internucleotide H3′(i−1)−P(i) connectivities are labeled with the nucleotide containing the H3′(i−1).

Phosphorus assignments were made from H3′−P correlation cross-peaks in the $^{1}H-^{31}P$ HETCOR spectra (Figure 6). Except for 3′-P of U5 and A6, resonances are within a 1.1 ppm region. The U5−3′P (−0.86 ppm) and A6−3′P (−1.93 ppm) are shifted downfield. The correlation between phosphorus chemical shifts and backbone torsion angles proposed by Gorenstein et al. (1984, 1988) indicates that the turn in the hairpin involves the U5 and A6 nucleotides.

Coupling Constant and Torsion Angle Analysis. It is known that the $J_{H1'-H2'}$ and $J_{H3'-H4'}$ coupling values have an inverse relationship (v. d. Ven & Hilbers, 1988). In a C2′-endo sugar conformation, the $J_{H1'-H2'}$ coupling is large (∼10 Hz) and the $J_{H3'-H4'}$ coupling is small (<2 Hz). The opposite is true for a C3′-endo conformation. In A-form RNA, the sugar conformation is predominantly C3′-endo, which results in a small $J_{H1'-H2'}$ coupling constant (<1.5 Hz). In most cases, the $J_{H1'-H2'}$ coupling is not observed for C3′-endo sugars due to line-width cancellation of antiphase cross-peaks in DQF-COSY spectra. The measured J-coupling values for the hairpin are listed in Table 2 and the dihedral angle restraints in Table 3. In the DQF-COSY spectrum recorded at 35 °C, the $J_{H1'-H2'}$ coupling values for the six nucleotides in the loop are large (4−8 Hz), suggesting that they have a high percentage of C2′-endo conformers in solution. In the DQF-COSY spectrum recorded at 25 °C, the $J_{H1'-H2'}$ correlation cross-peaks for A6 and A7 are still present, the G4 and A9 are weak, and the U5 and U8 are no longer observed. The lack of U5 and U8 $J_{H1'-H2'}$ coupling cross-peaks may be due in part to the slowed conformational motion at 25 °C, or a shift in the C3′-endo to C2′-endo equilibrium for these sugars. In the DQF-COSY spectra recorded at both 35 and 25 °C, the $J_{H3'-H4'}$ couplings are large (∼10 Hz) for all measurable $J_{H3'-H4'}$ coupling cross-peaks, suggesting that these sugars are in a C3′-endo

Table 2: Proton−Proton and Proton−Phosphorus Coupling Constants for the r(GGCGUAAUAGCC) Hairpin[a]

	H1′−H2′	H2′−H3′	H3′−H4′	H3′−P
G1	4 (4)	5	10 (11)	11
G2	<3 (<3)	*b*	9 (10)	*c*
C3	<3 (<3)	5	10 (9)	12
G4	3 (4)	6	9 (9)	10
U5	<3 (6)	5	11 (12)	11
A6	3 (4)	5	10 (9)	12
A7	3 (5)	5	9 (9)	11
U8	<3 (8)	5	12 (*b*)	10
A9	5 (6)	5	12 (10)	12
G10	*b* (*b*)	*b*	*b* (*b*)	*c*
C11	<3 (5)	*b*	*b* (8)	*c*
C12	5 (4)	5	*b* (10)	

[a] *J*-coupling values were obtained from a ^{31}P decoupled DQF-COSY spectrum recorded at 25 °C. [b] Coupling could not be determined due to overlap. [c] H3′−P coupling could not be obtained due to unmeasurable H2′−H3′ *J*-coupling. *J*-coupling values measured at 35 °C are in parentheses.

Table 3: Dihedral Angle Restraints for r(GGCGUAAUAGCC)[a]

nucleotide	α	ν_1	δ	ϵ	ζ
G1	0 ± 120	−15 ± 30	80 ± 20	−130 ± 40	0 ± 120
G2	0 ± 120	−15 ± 30	80 ± 20	*b*	0 ± 120
C3	0 ± 120	−15 ± 30	80 ± 20	−130 ± 40	0 ± 120
G4	0 ± 120		80 ± 30	−130 ± 40	0 ± 120
U5			80 ± 30	−130 ± 40	
A6	0 ± 120		80 ± 30	−130 ± 40	0 ± 120
A7	0 ± 120		80 ± 30	−130 ± 40	0 ± 120
U8	0 ± 120			−130 ± 40	0 ± 120
A9	0 ± 120		80 ± 30	−120 ± 40	0 ± 120
G10	0 ± 120			*b*	0 ± 120
C11	0 ± 120	−15 ± 30	80 ± 20	−130 ± 40	0 ± 120
C12		−15 ± 60		*b*	

[a] Torsion angles were determined from *J*-coupling data in ^{31}P decoupled DQF-COSY spectra recorded at 25 °C. [b] H3′−P coupling could not be determined due to spectral overlap of the H2′−H3′ cross-peak.

geometry. The large $J_{H1'-H2'}$ and $J_{H3'-H4'}$ coupling for the loop sugars at 35 °C indicates that the loop is undergoing dynamic interconversion between C2′-endo and C3′-endo conformers (Jaeger & Tinoco, 1993).

H3′−P coupling constants were obtained by subtracting the passive $J_{H2'-H3'}$ coupling from $J_{H3'-P}$ values measured in a ^{31}P−^{1}H HETCOR spectrum (Varani & Tinoco, 1991). The $J_{H3'-P}$ coupling values are similar to one another, indicating no large changes in the ϵ torsion angles in the hairpin. The dynamic nature of the U5, A6, A7, and U8 sugars suggests that the $J_{H3'-P}$ coupling may be affected by conformational averaging. Therefore, the ϵ torsion angles were given bounds of ±40° in order to accommodate conformational averaging.

Key NOE Interactions. There are key NOEs that determine the G4 and A9 base pairing, characterize the U5 and U8 bases in the loop, and define the turning point in the hairpin. Two NOEs characterize the G4 and A9 base-pairing scheme. A weak cross strand NOE between G4-H1′ and A9-H2 (cross-peak h in Figure 5) places the A9-H2 closer to the G4 sugar than in A-form RNA. An NOE between the A9-H2 and G10-H1′ (cross-peak i in Figure 5 and E in Figure 7) and the upfield chemical shift observed for the G10-H1′ suggest that the A9 base is above the G10 sugar, thus shielding the G10-H1′. These NOEs and chemical shift arguments lead to the conclusion that G4 and A9 adopt a sheared base pair orientation as shown in Figure 1. The

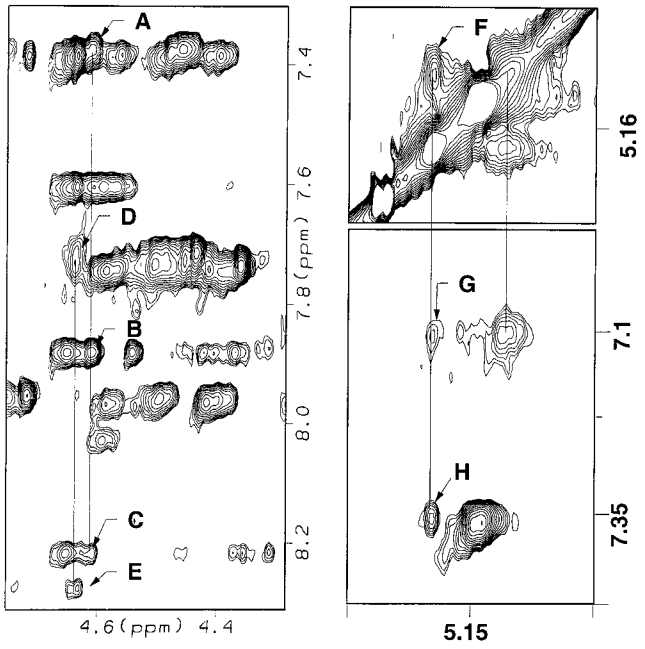

FIGURE 7: Portions of the 600 ms NOESY spectrum recorded at 25 °C in D_2O. Cross-peaks are as follows: (A) U5-H6 to U5-H2′, (B) A7-H8 to U5-H2′, (C) A6-H8 to U5-H2′, (D) G10-H1′ to G10-H8 and C11-H6, (E) A9-H2 to G10-H1′, (F) U5-H1′ to U8-H5, (G) U5-H1′ to U8-H6, and (H) U5-H1′ to U5-H8.

chemical shift of the G4 imino proton is also consistent with this structure (Heus & Pardi, 1991; SantaLucia & Turner, 1993; Walter et al., 1994).

In the loop, U5-H1′ exhibits cross-strand NOEs to U8-H5 and U8-H6 (cross-peaks F and G in Figure 7). In order for these NOE interactions to occur, U8 must have its H5 and H6 protons oriented toward the U5 sugar. This results in the U8 (NH) imino proton facing away from the U5 base. These strong NOEs rule out formation of hydrogen bonds between the U5 and U8 bases. Thus, U8 and U5 cannot be in a U·U mismatch involving hydrogen bonding of the imino protons. The U5-H2′ proton exhibits NOEs to both A6-H8 and A7-H8 (cross-peaks B and C in Figure 7), suggesting that the turn in the helix is at U5 and A6. Supporting evidence for the turning point in the helix is the large downfield shifts of the 3′-P of U5 and A6.

Distance Restraints. There were a total of 66 NOE-derived distance restraints and 9 hydrogen bond restraints used in determining the structural features of the r(GGCGUAAUAGCC) hairpin. The nine hydrogen bond restraints, determined from NOE interactions observed in one- and two-dimensional experiments, defined the three G·C base pairs in the stem.

The nonexchangeable proton−proton distance restraints were determined from a 120 ms NOESY spectrum using the C11 and C12 H5−H6 cross-peak volumes referenced to 2.45 Å (see Materials and Methods). The upper and lower bounds are shown in Table 4. Any distance that was greater than 5 Å had a lower bound of 4 Å and an upper bound of 6.5 Å. Several distances in the final average structure are beyond the distance restraint bounds (see Table 4). The violation of these distances may be attributed to conformational exchange.

Structural Analysis. Thirty structures were calculated as described in Materials and Methods, and representative structures are shown in Figure 8. The structures ranged from

Table 4: Distance Restraints (Å) for the r(GGCGUAAUAGCC) Hairpin[a]

atom 1	atom 2	lower	upper	distance	atom 1	atom 2	lower	upper	distance
G1-H1′	G2-H8	3.5	5.0	4.9	U5-H3′	U5-H6	2.0	3.2	2.5
G1-H1′	G1-H8	3.3	4.1	3.7	U5-H6	A6-H8	4.0	10.0	7.3
G1-H2′	G1′H8	3.9	5.7	4.1	A6-H1′	A7-H8	3.2	4.6	5.1[b]
G1-H2′	G2-H8	1.9	2.8	2.4	A6-H1′	A6-H8	3.5	4.1	3.6
G1-H3′	G1-H8	2.8	4.0	3.3	A6-H2′	A6-H8	2.2	4.0	4.4[b]
G2-H1′	C3-H6	4.6	6.6	5.1	A6-H2′	A7-H8	2.8	4.0	2.7[b]
G2-H1′	G2-H8	3.3	4.1	3.8	A6-H2′	A6-H1′	2.4	3.5	2.8
G2-H2′	G2-H8	2.1	4.2	4.0	A6-H3′	A6-H8	3.2	4.6	3.4
G2-H2′	C3-H6	1.8	2.6	2.7[b]	A6-H8	A7-H8	3.5	6.5	4.9
G2-H2′	G2-H1′	2.4	3.5	2.8	A7-H1′	A6-H2	3.2	4.6	3.1[b]
G2-H8	C3-H6	3.5	6.5	4.8	A7-H1′	A7-H8	2.9	4.1	3.8
C3-H1′	C3-H6	3.0	4.1	3.6	A7-H1′	A7-H2	3.6	5.2	4.7
C3-H1′	G4-H8	4.0	6.5	5.1	A7-H2′	A7-H8	2.8	4.1	4.0
C3-H2′	G4-H8	2.1	3.1	2.8	A7-H2′	A7-H1′	2.5	3.6	2.7
C3-H2′	C3-H6	3.0	4.3	4.1	A7-H2′	U8-H6	2.9	4.2	2.9
C3-H2′	C3-H1′	2.2	3.2	2.8	A7-H3′	A7-H8	2.4	3.4	2.8
C3-H3′	C3-H6	2.2	3.1	3.0	A7-H4′	A7-H1′	3.0	6.5	3.3
C3-H3′	G4-H8	2.2	3.2	2.9	U8-H1′	A7-H2	3.5	6.0	3.0
C3-H5	G4-H8	4.0	6.5	4.8	U8-H1′	U8-H6	3.2	4.1	3.6
C3-H5	G2-H8	4.0	6.5	4.5	U8-H2′	U8-H6	2.6	3.8	4.1[b]
G4-H1′	U5-H6	4.0	6.5	4.5	U8-H5	U5-H2′	3.0	5.0	4.7
G4-H1′	G4-H8	3.0	4.3	3.8	A9-H1′	A9-H8	3.1	4.1	3.8
G4-H1′	A9-H2	4.0	6.5	6.6[b]	A9-H2′	A9-H1′	2.2	3.1	2.7
G4-H2′	U5-H6	2.2	3.1	2.2	A9-H3′	A9-H8	2.6	3.8	2.8
G4-H2′	G4-H8	2.4	3.5	3.7[b]	G10-H1′	A9-H2	3.5	6.0	4.1
G4-H2′	G4-H1′	2.3	3.3	2.8	G10-H3′	G10-H8	3.0	4.4	3.9
G4-H3′	G4-H8	2.1	3.0	2.8	G10-H3′	C11-H6	2.0	3.1	3.0
G4-H8	C3-H6	3.5	6.5	4.5	C11-H2′	C12-H6	1.9	3.2	2.3
U5-H1′	U5-H6	2.6	4.1	3.7	C11-H2′	C11-H1′	2.2	3.2	2.8
U5-H1′	U8-H6	3.5	6.5	5.2	C12-H1′	C12-H6	3.2	4.1	3.6
U5-H1′	U8-H5	2.5	4.5	3.5	C12-H2′	C12-H1′	2.3	3.4	2.8
U5-H2′	U5-H6	2.2	4.0	3.7	C12-H2′	C12-H6	2.5	5.6	3.9
U5-H2′	A7-H8	3.0	4.5	2.9[b]	C12-H5	C12-H1′	4.0	6.5	5.4

[a] Measured distance is from the minimized average structure (Figure 8). [b] Distance outside of restraint bounds.

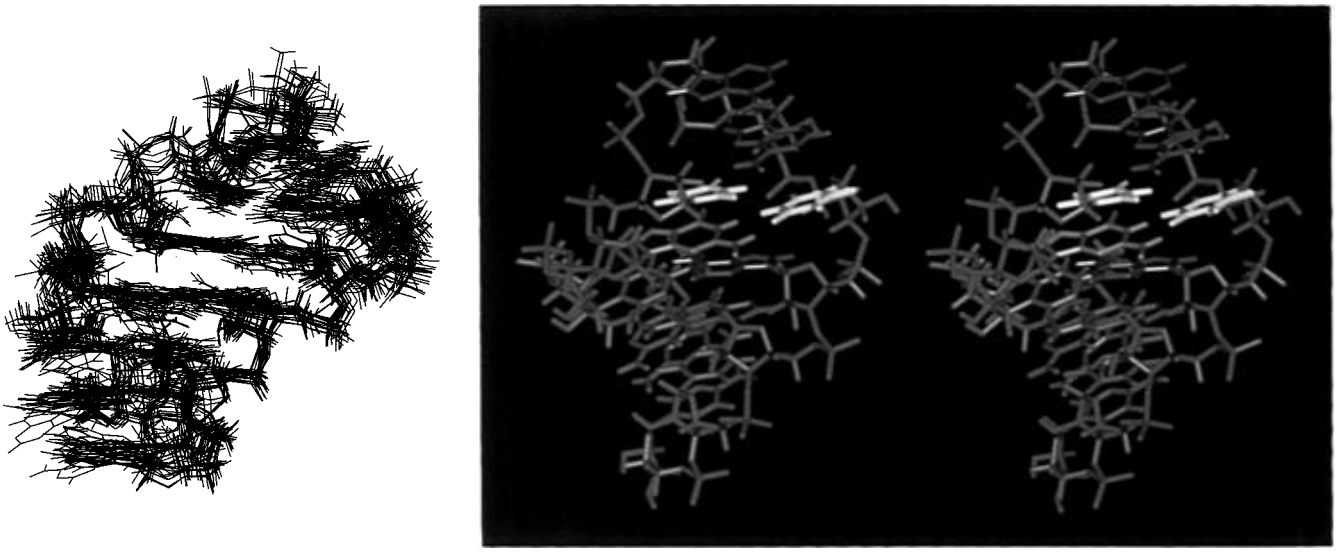

FIGURE 8: Structures generated for the r(GGCGUAAUAGCC) hairpin using restrained molecular dynamics and energy minimization. (Left) Superposition of structures generated using the method described in the text. (Right) Stereo image of the energy-minimized structure of the average of all calculated structures. The stem bases and phosphate backbone are blue, the G4 base is green, the A6, A7, and A9 bases are red, and the U5 and U8 bases are yellow. The average structure has a hydrogen bond from the U5 imino proton to the phosphate between A7 and U8. Some structures, however, had a hydrogen bond from the G4 imino proton to the phosphate between A7 and U8.

−60 to −80 kcal/mol in energy. An overlay of the GA mismatches is shown in Figure 9. The structures exhibit general features. The G4 and A9 bases adopt a sheared GA base pair similar to those previously reported in both RNA (Heus & Pardi, 1991; SantaLucia & Turner, 1993; Ebel et al., 1994; Biou et al., 1994) and DNA (Li et al., 1991; Cheng et al., 1992; Maskos et al., 1993). As shown in Figure 9, however, the structure of the GA mismatch is fluxional. This is not surprising. The GA mismatches observed in GA_3 tetraloops by NMR (Heus & Pardi, 1991) and X-ray crystallography (Pley et al., 1994b) have slightly different hydrogen-bonding schemes, and a thermodynamic study of a GCAA tetraloop suggests individual hydrogen-bonding groups do not contribute much to stability (SantaLucia et al., 1992).

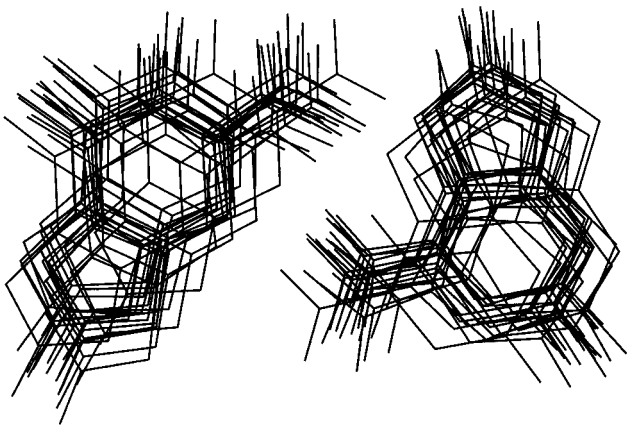

FIGURE 9: Superposition of GA mismatches from structures generated.

The U8 of the loop is positioned such that the U8-H5 and U8-H6 protons are located in the interior of the loop, leaving the U8 hydrogen-bonding groups exposed to the solvent. The U5 base is stacked on the G4·A9 mismatch with the U5 imino proton oriented toward the interior of the loop. The turn in the helix involves the phosphodiester linkage between the U5 and A6 nucleotides. The U5 imino proton is close to the A7 phosphate group so that a hydrogen bond can form, creating a uridine turn motif (see Figure 8B). The G4 imino proton is sufficiently far away from the opposite phosphate group that a direct hydrogen bond cannot form. If a water molecule was halfway between the phosphate and the G4 imino proton, however, a water-bridged hydrogen bond could occur. The A6 and A7 bases are stacked on one another, with U8 often stacked on A7. This may allow for proper alignment for hydrogen bond formation with a complementary sequence, thus forming a pseudoknot. While the above features are usually present in the structures generated, the loop appears able to adopt more than a single conformation (Figure 8A).

DISCUSSION

Although the GUAAUA loop is apparently not rigid, two previously observed RNA motifs characterize this loop: formation of a sheared GA mismatch and the presence of a uridine turn. The G4 and A9 bases form a hydrogen-bonded mismatch in a sheared conformation (see Figure 1) as observed for GNRA tetraloops (Heus & Pardi, 1991; Pley et al., 1994b). The UAA sequence can form a uridine turn similar to that in the anticodon and TΨC hairpin loops in tRNA (Kim & Sussman, 1976; Quigley & Rich, 1976) and in the hammerhead ribozyme (Pley et al., 1994a). The UAA sequence is consistent with the UNR (R is purine) consensus sequence for a uridine turn suggested by Pley et al. (1994a). The hydrogen bond between the U5 imino and A7 phosphate is not observed in every structure, suggesting it is fluxional and may sometimes be mediated by a water molecule.

The structural features of the GUAAUA hairpin loop are important for two reasons. They provide insight into the thermodynamic parameters measured for similar hairpin loops of six nucleotides (Serra et al., 1994, 1993). They also provide a foundation for eventually understanding structure−function relationships of this conserved hairpin loop in the ribosome.

The structural data support a previous model for predicting the stability for RNA hairpins where the loop size, closing base pairs, and the interactions of the first mismatch are the primary factors determining hairpin stability (Serra et al., 1994). In this model, the first mismatch is assumed to be stacked on the closing base pair, and an additional 0.7 kcal/mol favorable free energy increment is assigned for a GA mismatch. The stacking and hydrogen-bonding interactions of the GA mismatch are consistent with this model. In particular, the sheared GA mismatch has previously been observed in the hairpin loops GCAA and GAAA (Heus & Pardi, 1991; Pley et al., 1994b) and a 0.7 kcal/mol increment assigned to the hydrogen bonding interactions (SantaLucia et al., 1992). Both this work and comparison of the different GNRA tetraloop structures determined by NMR (Heus & Pardi, 1991) and X-ray crystallography (Pley et al., 1994b) suggest the hydrogen bonds in the sheared GA mismatch may be fluxional.

The lack of hydrogen bonding between the U5 and U8 bases indicates the second mismatch is not formed and does not contribute to the stability of the hairpin. Thermodynamic stabilities of C(A_n)G and C(U_n)G hairpins where $n = 4$, 5, and 7 show that the U_n hairpins are 0.4 kcal/mol more stable (Groebe & Uhlenbeck, 1988). This difference is small when compared to the possible number of hydrogen-bonded UU mismatches that can occur in the $n = 5$ and 7 loops. It is consistent, however, with formation of a single hydrogen bonded U·U (Serra et al., 1994). The U_9 loop, however, is 2.4 kcal/mol more stable than the A_9 loop, suggesting that more than one of the UU mismatches is base paired. This suggests that secondary mismatch interactions may not be important for loop sizes less that eight nucleotides but may be important for larger loop sizes. A recent NMR structure of a hairpin with a 17-nucleotide loop exhibits many non-Watson−Crick base pairs (Szewczak et al., 1993).

The r(GGCGUAAUAGCC) hairpin loop structure with the A6, A7, and U8 bases stacked on the 3′ side of the loop is consistent with previous suggestions that stacking is preferred on the 3′ side of an RNA loop (Haasnoot et al., 1986; Jaeger & Tinoco, 1993; Michnicka et al., 1993; Pardi, 1994; Puglisi et al., 1990). It has been hypothesized that the constraints imposed by the loop may affect the base stacking within the loop (Haasnoot et al., 1986).

The NMR data show that the loop is flexible and is undergoing interconversion between two or more structures in solution. This is expected from theoretical considerations (Marky & Olson, 1987). The flexibility is evident in the temperature studies and in the observed large $J_{H1'-H2'}$ and $J_{H3'-H4'}$ couplings in the loop sugars, particularly at 35 °C. In the six-nucleotide loop of the HIV-1 TAR element hairpin r(GAGCCUGGGAGCUC), conformational interconversion between multiple structures also occurs (Colvin et al., 1993; Michnicka et al., 1993; Jaeger & Tinoco, 1993). From the structural calculations on the r(GGCGUAAUAGCC) hairpin and the NMR data, it appears that this loop is more ordered than that of the six-nucleotide HIV-1 TAR element hairpin (Colvin et al., 1993; Michnicka et al., 1993; Jaeger & Tinoco, 1993). This may be due in part to the additional constraints imposed by the sheared GA base pair. The sheared GA base pair compresses the helix, thus imposing constraints on the phosphate backbone that would be absent with the unpaired CA mismatch in the TAR element hairpin.

Biological Implications. The structure of the GUAAUA hairpin loop leaves the sequence AAU on the solvent-exposed side of the loop for interaction with either RNA or

protein. Thus AAU is presented much like the anticodon of tRNA. The loop is also flexible so that it has possibilities for binding to receptors in an induced-fit manner. The true significance of the GUAAUA loop structure will presumably be revealed when structural information becomes available for its partners in binding.

Comparison to Huang et al. (1996). While our manuscript was in review, we received a preprint of a paper by Huang et al. (1996) reporting the structure for the GUAAUA hairpin loop at 25 °C in 35 mM Na^+, pH 6.0, in the contexts GGGCGUAAUAGCCC and GGACGUAAUAGUCC. The main structural conclusions from their work are similar to those reported here. They find the GA mismatch in a sheared conformation followed by a U-turn. Their conclusions differ from those reported here in that they report a single, well-defined conformation with the second U unstructured and on the outside of the loop. We report a more flexible loop with the second U often stacked. These different interpretations apparently reflect real differences in the NMR data, suggesting the flexibility and structure of this loop are sensitive to either the number of base pairs in the stem or the buffer conditions. The combined results suggest there are interesting subtle factors that partially control RNA structure and energetics.

ACKNOWLEDGMENT

We thank Dr. David E. Draper for sending a preprint of the manuscript reporting structures for GGGCGUAAUAGCCC and GGACGUAAUAGUCC.

SUPPORTING INFORMATION AVAILABLE

One figure showing a plot of inverse melting temperature vs oligomer concentration and one figure showing a 600 ms NOESY spectrum (2 pages). Ordering information is given on any current masthead page.

REFERENCES

Altman, S. (1990) *J. Biol. Chem. 265*, 20053−20056.
Biou, V., Yaremchuk, A., Tukalo, M., & Cusack, S. (1994) *Science 263*, 1404−1410.
Borer, P. N., Lin, Y., Wang, S., Roggenbuck, M. W., Gott, J. M., Uhlenbeck, O. C., & Pelczer, I. (1995) *Biochemistry 34*, 6488−6503.
Cech, T. R. (1990) *Annu. Rev. Biochem. 59*, 543−568.
Cheng, J.-W., Chou, S.-H., & Reid, B. R. (1992) *J. Mol. Biol. 228*, 1037−1041.
Cheong, C., Varani, G., & Tinoco, I., Jr. (1990) *Nature 346*, 680−682.
Colvin, R. A., White, S. W., Garcia-Blanco, M. A., & Hoffman, D. W. (1993) *Biochemistry 32*, 1105−1112.
Cornell, W. D., Cieplak, P., Bayly, C., Gould I. R., Merz, K. M., Jr., Ferguson, D. M., Spellmeyer, D. C., Fox, T., Caldwell, J. W., & Kollman, P. A. (1995) *J. Am. Chem. Soc. 117*, 5179−5197.
Ebel, S., Brown, T., & Lane, A. N. (1994) *Eur. J. Biochem. 220*, 703−715.
Freier, S. M., Burger, B. J., Alkema, D., Neilson, T., & Turner, D. H. (1983) *Biochemistry 22*, 6198−6206.
Gautheret, D., Major, F., & Cedergren, R. (1993) *J. Mol. Biol. 229*, 1049−1064.
Gorenstein, D. G., & Luxon, B. A. (1984) *Phosphorous-31 NMR: Principles and Applications*, Academic Press, New York.
Gorenstein, D. G., Schroeder, S. A., Fu, J. M., Metz, J. T., Roongta, V., & Jones, C. R. (1988) *Biochemistry 27*, 7223−7237.
Groebe, D. R., & Uhlenbeck, O. C. (1988) *Nucleic Acids Res. 16*, 11725−11735.
Gutell, R. R. (1994) *Nucleic Acids Res. 22*, 3502−3507.
Gutell, R. R., Gray, M. W., & Schnare, M. N. (1993) *Nucleic Acids Res. 21*, 3055−3074.
Gutell, R. R., Larsen, N., & Woese, C. R. (1994) *Microbiol Rev. 58*, 10−26.
Haasnoot, C. A. G., Leeuw, F. A. A. M. d., & Altona, C. (1980) *Tetrahedron 36*, 2783−2792.
Haasnoot, C. A. G., Hilbers, C. W., van der Marel, G. A., van Boom, J. H., Singh, U. C., Pattabiraman, N., & Kollman, P. A. (1986) *J. Biomol. Struct. Dyn. 3*, 843−857.
Heus, H. A., & Pardi, A. (1991) *Science 253*, 191−194.
Huang, S., Wang, Y.-X., & Draper, D. E. (1996) *J. Mol. Biol.* (in press).
Jaeger, J. A., & Tinoco, I. (1993) *Biochemistry 32*, 12522−12530.
Kim, S. H., & Sussman, J. L. (1976) *Nature 260*, 645−646.
Kim, S. H., Suddath, F. L., Quigley, G. J., McPherson, A., Sussman, J. L., Wang, A. H. J., Seeman, N. C., & Rich, A. (1974) *Science 185*, 435−440.
Lankhorst, P. P., Haasnoot, C. A. G., Erkelens, C., & Altona, C. (1984) *J. Biomol. Struct. Dyn. 1*, 1387−1405.
Li, Y., Zon, G., & Wilson, W. D. (1991) *Proc. Natl. Acad. Sci. U.S.A. 88*, 26−30.
Luan, D. D., Korman, M. H., Jakubczak, J. L., & Eickbush, T. H. (1993) *Cell 72*, 595−605.
Marky, N. L., & Olson, W. K. (1987) *Biopolymers 26*, 415−438.
Maskos, K., Gunn, B. M., LeBlanc, D. A., & Morden, K. M. (1993) *Biochemistry 32*, 3583−3595.
Michel, F., & Westhof, E. (1990) *J. Mol. Biol. 216*, 585−610.
Michnicka, M. J., Harper, J. W., & King, G. C. (1993) *Biochemistry 32*, 395−400.
Nikonowicz, E. P., & Pardi, A. (1992) *Nature 355*, 184−186.
Nikonowicz, E. P., & Pardi, A. (1993) *J. Mol. Biol. 232*, 1141−1156.
Pace, N. R., & Brown, J. W. (1995) *J. Bacteriol. 177*, 1919−1928.
Pardi, A. (1994) *Nat. Struct. Biol. 1*, 846−849.
Petersheim, M., & Turner, D. H. (1983) *Biochemistry 22*, 256−263.
Pley, H. W., Flaherty, K. M., & McKay, D. B. (1994a) *Nature 372*, 68−74.
Pley, H. W., Flaherty, K. M., & McKay, D. B. (1994b) *Nature 372*, 111−113.
Puglisi, J. D., Wyatt, J. R., & Tinoco, I., Jr. (1990) *Biochemistry 29*, 4215−4226.
Puglisi, J. D., Tan, R., Calnan, B. J., Frankel, A. D., & Williamson, J. R. (1992) *Science 257*, 76−80.
Quigley, G. J., & Rich, A. (1976) *Science 194*, 796−806.
Robertus, J. D., Ladner, J. E., Finch, J. T., Rhodes, D., Brown, R. D., Clark, B. F. C., & Klug, A. (1974) *Nature 250*, 546−551.
SantaLucia, J., Jr., & Turner, D. H. (1993) *Biochemistry 32*, 12612−12623.
SantaLucia, J., Jr., Kierzek, R., & Turner, D. H. (1991) *Biochemistry 30*, 8242−8251.
SantaLucia, J., Jr., Kierzek, R., & Turner, D. H. (1992) *Science 256*, 217−219.
Scott, W. G., Finch, J. T., & Klug, A. (1995) *Cell 81*, 991−1002.
Serra, M. J., & Turner, D. H. (1995) *Methods Enzymol. 259*, 242−261.
Serra, M. J., Lyttle, M. H., Axenson, T. J., Schadt, C. A., & Turner, D. H. (1993) *Nucleic Acids Res. 21*, 3845−3849.
Serra, M. J., Axenson, T. J., & Turner, D. H. (1994) *Biochemistry 33*, 14289−14296.
Singh, U. C., Weiner, P. K., Caldwell, J., & Kollman, P. C. (1988) *AMBER*, University of California, San Francisco.
Sklenar, V., & Bax, A. (1987) *J. Magn. Reson. 74*, 469−479.
Sklenar, V., Miyashio, H., Zon, G., Miles, H. T., & Bax, A. (1986) *FEBS Lett. 208*, 94−98.
Szewczak, A. A., Moore, P. B., Chan, Y.-L., & Wool, I. G. (1993) *Proc. Natl. Acad. Sci. U.S.A. 90*, 9581−9585.
Turner, D. H., Sugimoto, N., & Freier, S. M. (1988) *Annu. Rev. Biophys. Biophys. Chem. 17*, 167−192.
Usman, N., Ogilvie, K. K., Jiang, M. Y., & Cedergren, R. J. (1987) *J. Am. Chem. Soc. 109*, 7845−7854.
van de Ven, F. J. M., & Hilbers, C. W. (1988) *Eur. J. Biochem. 178*, 1−38.
Varani, G., & Tinoco, I., Jr. (1991) *Q. Rev. Biophys. 24*, 479−532.

Varani, G., Cheong, C., & Tinoco, I., Jr. (1991) *Biochemistry 30*, 3280−3289.
Walter, A. E., Wu, M., & Turner, D. H. (1994) *Biochemistry 33*, 11349−11354.
Walter, P., & Blobel, G. (1982) *Nature 299*, 691−698.
Walter, P., & Johnson, A. E. (1994) *Annu. Rev. Cell Biol. 10*, 87−119.
Weiner, P. K., & Kollman, P. A. (1981) *J. Comput. Chem. 2*, 287−303.
Weiner, S. J., Kollman, P. A., Case, D. A., Singh, U. C., Ghio, C., Alagona, G., Profeta, S., Jr., & Weiner, P. (1984) *J. Am. Chem. Soc. 106*, 765−784.
Weiner, S. J., Kollman, P. A., Nguyen, D. T., & Case, D. A. (1986) *J. Comput. Chem. 7*, 230−252.
Westhof, E., Dumas, P., & Moras, D. (1985) *J. Mol. Biol. 184*, 119−145.
Wimberly, B., Varani, G., & Tinoco, I., Jr. (1993) *Biochemistry 32*, 1078−1087.
Woese, C. R., & Pace, N. R. (1993) in *The RNA World* (Gesteland, R. F., & Atkins, J. F., Eds.) pp 91−117, Cold Spring Harbor Press, Cold Spring Harbor, NY.
Woese, C. R., Winker, S., & Gutell, R. R. (1990) *Proc. Natl. Acad. Sci. U.S.A. 87*, 8467−8471.
Wu, M., McDowell, J. A., & Turner, D. H. (1995) *Biochemistry 34*, 3204−3211.
Wüthrich, K. (1986) *NMR of Proteins and Nucleic Acids*, John Wiley and Sons, New York.
Xing, Y. Y., & Draper, D. E. (1995) *J. Mol. Biol. 249*, 319−331.
Zuker, M. (1989) *Science 244*, 48−52.

BI952697K